Available online at www.sciencedirect.com
ScienceDirect
Catalysis Today 127 (2007) 176–188
CATALYSIS TODAY
www.elsevier.com/locate/cattod

Characterization of Pd-based FCC CO/NO_x control additives by in situ FTIR and extended X-ray absorption fine structure spectroscopies

Oleg S. Alexeev [a], Sundaram Krishnamoorthy [b], Michael S. Ziebarth [b], George Yaluris [b], Terry G. Roberie [b], Michael D. Amiridis [a,*]

[a] *Department of Chemical Engineering, University of South Carolina, Columbia, SC 29208, United States*
[b] *GRACE Davison Refining Technologies, Columbia, MD 21044, United States*

Available online 6 July 2007

Abstract

$Pd^{n+}/Ce^{n+}/Na^{+}/\gamma$-$Al_2O_3$-type materials used as FCC additives for CO/NO_x control were characterized by extended X-ray absorption fine structure (EXAFS) spectroscopy and in situ FTIR. The EXAFS data indicate that in freshly prepared samples palladium is present in the form of highly dispersed PdO species. Reduction with H_2 at 500 °C leads to the formation of small Pd clusters incorporating on average approximately six to eight metal atoms at a Pd−Pd bond distance of 2.76 Å. All components of these materials can interact with NO and promote the formation of nitrate/nitrite species, essentially ''trapping'' NO_x species on the catalyst surface. However, the Na^+ species dominate the surface chemistry and readily form sodium nitrates with a characteristic IR band at 1370–1385 cm^{-1}. Finally, hydroxyls from the support are also actively participating in the formation of HNO_x type compounds with characteristic stretching vibrations in the 3500–3572 cm^{-1} region.

Keywords: EXAFS; FTIR; FCC additive; Palladium; NO adsorption; NO_x reduction

1. Introduction

Fluid catalytic cracking (FCC) is the primary hydrocarbon conversion/molecular reduction process in modern petroleum refineries. Approximately, 35–40% of the total gasoline production in a typical refinery comes from the FCC unit [1,2]. The ability to convert a variety of feed types (e.g., gas oil, atmospheric and vacuum residue) into lighter and more valuable products, such as gasoline/diesel and light olefins, makes the FCC process extremely versatile. In a typical FCC process, feedstock hydrocarbons are cracked into lighter molecules in the riser reactor, while coke is deposited on the catalyst. The coke contains nitrogen, the level of which depends mainly on the content and type of nitrogen molecules in the feedstock. During the subsequent regeneration of the catalyst, the coke is burned off and a portion of its nitrogen is released as NO_x. Therefore, along with the desirable products, a number of gaseous pollutants are also formed in the FCC process during the regeneration of the catalyst. It is estimated that the FCC regenerators are responsible for approximately 50% of the total NO_x emissions from refineries and approximately 10% of the overall NO_x emissions from stationary sources in the US [3]. Environmental regulations are currently in place to control NO_x emissions from refineries.

Extensive pilot plant studies conducted using the Davison Circulating Riser (a pilot scale adiabatic circulating riser with continuous catalyst regeneration, which is a very good simulator of a commercial FCC unit) have shown that approximately 35–45% of the nitrogen in the feed ends up in the coke formed during the cracking process [4,5]. Approximately, 90% of the nitrogen present in the coke exits the FCC regenerator in the form of N_2 following the regeneration process [4,5]. However, the remaining 10% can be emitted either as NO_x or reduced nitrogen species, depending upon the operating mode of the regenerator. FCC regenerators can operate in partial combustion or full combustion modes. In full combustion mode, the unit has sufficient amount of air to convert essentially all coke on the catalyst to CO_2 and H_2O, and the gas effluent exiting the regenerator contains typically between 0.5% and 4% of oxygen.

* Corresponding author. Tel.: +1 803 777 7356.
E-mail address: amiridis@engr.sc.edu (M.D. Amiridis).

0920-5861/$ – see front matter © 2007 Elsevier B.V. All rights reserved.
doi:10.1016/j.cattod.2007.05.016

In this type of operation, approximately 10% of the nitrogen present in the coke exits the regenerator as NO_x. When partial combustion mode is used, the unit has an insufficient amount of air for the complete oxidation of coke to CO_2 and H_2O. As a result, a significant percentage of coke is converted only to CO, while some also remains on the catalyst. Under these incomplete combustion conditions, the gaseous effluent exiting the regenerator consists of both oxidized and reduced N-containing species (i.e., NO_x, NH_3 and HCN) in addition to N_2, and should be treated further in a CO boiler where CO is converted to CO_2 and the reduced N-species are converted to NO_x. Therefore, the significant differences in the nature of the N-containing species formed during these two different modes of regenerator operation make the NO_x reduction concept in FCC units extremely challenging.

The approaches being investigated by the industry for NO_x reduction include: (a) the use of various additives in the circulating catalyst inventory capable of reducing NO_x emissions in situ, (b) process changes that would result in lower rates of NO_x formation and emission and (c) ex situ treatment of the exhaust gas using the selective catalytic reduction (SCR) or scrubbing methodologies. Among these strategies, the in situ additive approach has proven to be the most efficient and cost-effective approach in most cases. Pt-based combustion promoters are commonly used as additives to the circulating catalyst inventory in FCC units in order to reduce CO emissions from the regenerator [2]. However, these additives also convert N-containing coke species mainly to NO_x. Therefore, it is feasible that a successful reduction of NO_x can be achieved either with additives capable of reducing NO_x and operating independently from the Pt-based combustion promoters or with new additives capable of providing simultaneous reduction of both NO_x and CO emissions. In fact, both of these approaches are currently employed as industry-leading NO_x abatement solutions [6–11]. The NO_x reduction additives typically consist of supported transition metals. Such additives capable of promoting both the oxidation of CO and the reduction of NO_x are based on non-Pt noble metals supported on mixed oxide supports, with Al_2O_3 being the primary support component [6–11]. However, there is only a very limited number of literature reports outlining the NO_x reduction chemistry under FCC regenerator conditions [12–17]. Some of these reports have focused on the NO_x formation mechanism during the combustion of coke [12–15], while only few have focused on the investigation of the NO_x reduction by CO over Rh and Ir additives [16,17].

This report is the first in a series of systematic investigations aimed at understanding the mechanism of the NO reduction by CO over Pd-based catalysts under FCC regenerator conditions and it focuses on the characterization of $Pd^{n+}/Ce^{n+}/Na^{+}/\gamma$-$Al_2O_3$ type of materials. Extended X-ray absorption fine structure (EXAFS) and in situ FTIR spectroscopy measurements are therefore used to clarify the role of each component of such materials in the surface chemistry taking place during the interactions with NO under various conditions. The interaction of NO with CO over these materials is reported separately [18].

2. Experimental methods

2.1. Reagents and materials

An acid peptizable boehmite aluminum oxide hydroxide (Capital B, SASOL) was used as the alumina source. This material was calcined at 600 °C to produce γ-Al_2O_3 with a BET surface area of 200 m^2/g, which was used as the support. The palladium nitrate solution (99.95% purity), sodium hydroxide and cerium carbonate (99% purity) were obtained from Alfa Aesar, J.T. Baker and Rhone-Poulenc, respectively, and used as supplied. He (UHP grade, National Welders) was additionally purified prior to use by passage through an oxygen/moisture trap (Model OT3-2, Agilent) capable of removing traces of O_2 and water to 15 and 25 ppb, respectively. The NO/He, O_2/He and CO/He mixtures used (National Welders) were purified by passage through a moisture trap (Model GMT-2GCHP, Agilent) capable of removing water to 25 ppb.

2.2. Samples preparation

The Na^{+}/γ-Al_2O_3, Ce^{n+}/γ-Al_2O_3 and $Ce^{n+}/Na^{+}/\gamma$-Al_2O_3 materials were initially prepared as slurries and then spray-dried in a Bowen Spray dryer. Milling of slurries was carried out in a 4 L Drais mill. The spray-dried materials were subsequently calcined in air for 2 h at 538 °C. The nominal Na_2O and CeO_2 concentrations in the resulting materials were 7 and 20 wt.%, respectively.

The palladium containing samples were prepared by incipient wetness impregnation of the respective supports with aqueous solutions of palladium nitrate. In each case, the amount of the palladium precursor was chosen to yield samples containing approximately 1100 ppm of Pd. The samples were dried in air at 110 °C for 24 h and then calcined for 2 h at 538 °C.

2.3. FTIR spectroscopy

FTIR spectra were collected with a Nicolet Nexus 470 spectrometer equipped with a MCT-B detector cooled by liquid nitrogen. Powder samples (25 mg) were pressed into self-supported wafers having nearly the same density and thickness by applying 5000 psi of pressure. These wafers were subsequently mounted in the IR cell, which was connected to a gas distribution manifold. The design of the IR cell was similar to that described elsewhere [19]. Samples were pretreated in 10% O_2/He flow at the 400–600 °C temperature range for 2 h and then purged with He at the same temperature prior to each measurement. Spectra were recorded in the 300–400 °C temperature range at a spectral resolution of 2 cm^{-1} accumulating 64 scans per spectrum. The comparisons of infrared spectra for different samples were performed assuming that the extinction coefficient for a given adsorbed species remains unchanged from sample to sample.

2.4. EXAFS spectroscopy

EXAFS spectra were collected at beamline X-18B at the National Synchrotron Light Source (NSLS), Brookhaven

Table 1
EXAFS results at the Pd K-edge characterizing the $Pd^{n+}/Ce^{n+}/Na^{+}/\gamma\text{-}Al_2O_3$ sample after different treatments[a]

Treatment conditions	Shell	*N*	*R* (Å)	$\Delta\sigma^2$ (Å^2)	ΔE_0 (eV)	ε_v^2	k^1-variances (%)	
							Im.	Abs.
Fresh	Pd–Pd	–	–	–	–	1.2	3.04	1.04
	Pd–O	3.5	2.04	0.00350	−3.5			
H_2/500 °C	Pd–Pd	4.9	2.76	0.01000	3.1	0.9	1.47	0.67
	$Pd–O_{support}$							
	$Pd–O_s$	0.9	2.10	0.01000	−8.7			
	$Pd–O_l$	0.9	2.61	0.00150	−4.0			

[a] Notation: Standard deviations in fits: $N \pm 20\%$, $R \pm 1\%$, $\Delta\sigma^2 \pm 5\%$, $\Delta E_0 \pm 10\%$; *N*, coordination number; *R*, distance between absorber and backscatterer atoms; $\Delta\sigma^2$, the Debye-Waller factor, which is relative to the Debye-Waller factor of the reference compound; ΔE_0, the inner potential correction accounts for the difference in the inner potential between the sample and the reference compound; ε_v^2, goodness of fit. The subscripts s and l refer to short and long, respectively.

National Laboratory, Upton, NY, and at beamline 2–3 at the Stanford Synchrotron Radiation Laboratory (SSRL), Stanford Linear Accelerator Center, Menlo Park, CA. The storage ring electron energy was 2.8 GeV at NSLS and 3 GeV at SSRL. The ring currents were 110–250 and 80–100 mA at NSLS and SSRL, respectively.

The EXAFS data for $Pd^{n+}/Na^{+}/Ce^{n+}/\gamma\text{-}Al_2O_3$ samples were recorded in the fluorescence mode with a 13th element Ge detector. The total count rate for the Ge detector was in the range of 30,000–40,000 counts/s. It was experimentally established that the detector readings are linear within this range and no corrections for the dead-time are required. Spectra were collected for a freshly prepared sample, as well as a sample reduced with H_2 at 500 °C. After the H_2 reduction step was completed, the sample was purged with He at the reduction temperature, cooled down to room temperature in He flow and aligned in the X-ray beam. Data were then collected at room temperature with a Si(1 1 1) double-crystal monochromator that was detuned by 20% to minimize the effects of higher harmonics in the X-ray beam. The samples were scanned at energies near the Pd K absorption edge (24,350 eV).

The EXAFS data were analyzed with experimentally determined reference files obtained from EXAFS data characterizing materials of known structure. The Pd–Pd and $Pd–O_{support}$ interactions were analyzed with phase shifts and backscattering amplitudes obtained from EXAFS data for Pd foil and PdO, respectively. The crystallographic first-shell coordination parameters for all the reference compounds, the weighting of the Fourier transform, and the ranges in *k* and *r* space used to extract the reference functions from the experimental EXAFS data were reported previously [20]. The EXAFS parameters were extracted from the raw data with the aid of the XDAP software [21]. The methods used to extract the EXAFS function from raw data are essentially the same as those reported elsewhere [22]. The data used for each sample were the average of seven scans.

The data at the Pd K-edge obtained for the fresh $Pd/Na^{+}/Ce^{n+}/\gamma\text{-}Al_2O_3$ sample were analyzed with a maximum of four free parameters over the ranges of $3.9 < k < 15.0$ Å^{-1} (*k* is the wave vector) and $1.0 < r < 2.5$ Å (*r* is the distance from the absorbing atom; in this case Pd). The statistically justified number of free parameters, *n*, was found to be approximately 11, as estimated on the basis of the Nyquist theorem [23,24]: $n = (2\Delta k \Delta r/\pi) + 1$, where Δk and Δr, respectively, are the *k* and *r* ranges used in the data fitting. Similarly, the data at the Pd K-edge obtained for the reduced $Pd/Na^{+}/Ce^{n+}/\gamma\text{-}Al_2O_3$ sample were analyzed with a maximum of 12 free parameters over the ranges of $3.9 < k < 15.0$ Å^{-1} and $1.0 < r < 3.5$ Å. In this case, the statistically justified number of free parameters estimated as described above was found to be approximately 19. The parameters characterizing both the high-Z (Pd–Pd) and low-Z ($Pd–O_{support}$) contributions were determined by multiple-shell fitting in R-space with application of k^1 and k^3 weighting in the Fourier transformations [22]. The fit was optimized by use of a difference file technique with phase- and amplitude-corrected Fourier transforms of the data [25,26]. Standard deviations reported in Table 1 for various parameters were calculated from the covariance matrix taking into account the statistical noise of the EXAFS data and the correlations between the different coordination parameters as described elsewhere [27]. Systematic errors are not included in the calculation of the standard deviations. The values of the goodness of fit (ε_v^2) were calculated as outlined in the Reports on Standard and Criteria in XAFS Spectroscopy [28]. The variances in imaginary and absolute parts were used to determine the fit quality [29].

3. Results and discussion

3.1. Characterization of $Pd^{n+}/Ce^{n+}/Na^{+}/\gamma\text{-}Al_2O_3$ by EXAFS

The structural parameters determined from EXAFS data characterizing a freshly prepared $Pd^{n+}/Ce^{n+}/Na^{+}/\gamma\text{-}Al_2O_3$ sample, as well as a sample reduced with H_2 at 500 °C are summarized in Table 1. The raw EXAFS data characterizing the freshly prepared $Pd^{n+}/Ce^{n+}/Na^{+}/\gamma\text{-}Al_2O_3$ sample at the Pd K-edge show oscillations only up to a value of *k* (the wave vector) of approximately 11 Å^{-1} (Fig. 1A), indicating the presence of only low-Z backscatterers around the absorbing Pd atoms. The data analysis of this spectrum was performed assuming that Pd–O contributions are the best representatives of such low-Z backscatterers. When the Pd–O contributions thus calculated were subtracted from the spectrum, only noise was left in the residual spectrum (Fig. 1B), indicating that no other contributions need to be considered, and that the fit of the data with only Pd–O contributions included was satisfactory (Fig. 1C).

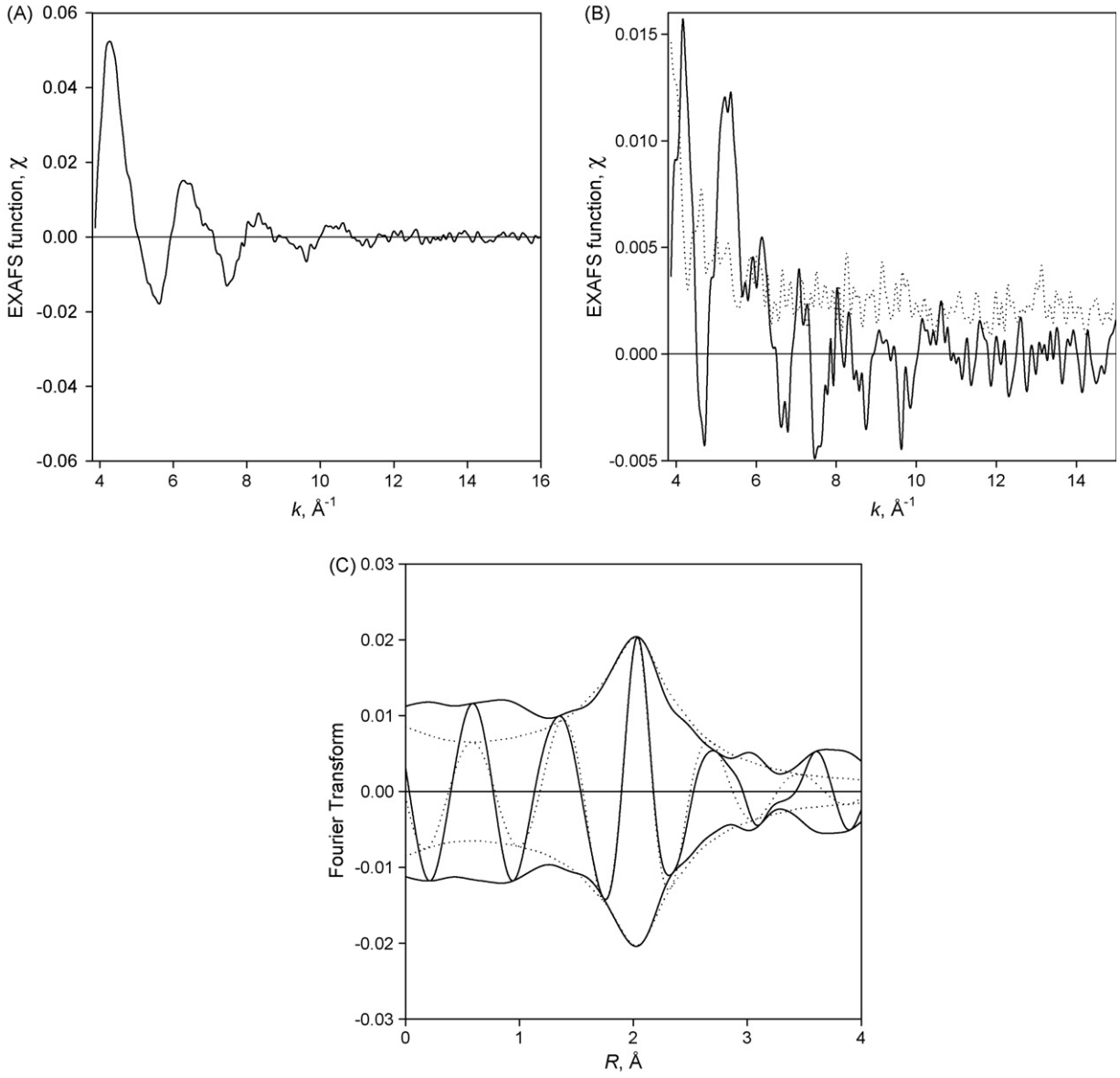

Fig. 1. (A) Experimental EXAFS (Chi) data of a fresh $Pd^{n+}/Ce^{n+}/Na^{+}/\gamma\text{-}Al_2O_3$ sample. (B) Residual spectrum (solid line) obtained after the subtraction of Pd−O contributions from the raw EXAFS data of a fresh $Pd^{n+}/Ce^{n+}/Na^{+}/\gamma\text{-}Al_2O_3$ sample and standard deviation (dotted line). (C) Imaginary part and magnitude of phase-corrected Fourier transform (k^0 weighted) of experimental EXAFS of a fresh $Pd^{n+}/Ce^{n+}/Na^{+}/\gamma\text{-}Al_2O_3$ sample (solid line) and calculated Pd–O contributions (dotted line).

Therefore, the optimized parameters for the Pd–O contributions indicate that each Pd atom has on average approximately 3.5 near oxygen neighbors at a bond distance of 2.04 Å (Table 1). These data are in close agreement with crystallographic data reported for palladium (II) oxide showing that in PdO each Pd atom has four adjacent oxygen atoms at a bond distance of 2.02 Å [30]. Therefore, we can conclude with a relatively high degree of confidence that Pd is present in the freshly prepared $Pd^{n+}/Ce^{n+}/Na^{+}/\gamma\text{-}Al_2O_3$ sample in the form of PdO. We should point out, however, that the EXAFS data do not allow us to distinguish whether the observed oxygen atoms belong to bulk PdO or to the different oxide components of the support.

In contrast, when the $Pd^{n+}/Ce^{n+}/Na^{+}/\gamma\text{-}Al_2O_3$ sample was reduced with H_2 at 500 °C, the raw EXAFS data collected at the Pd K-edge show oscillations up to a value of k of approximately 15 $Å^{-1}$ (Fig. 2A). Even though the oscillations observed in the high-k region were obviously weak, the existence of such oscillations is indicative of high-Z backscatterers in the neighborhood of Pd. Thus, after the first guess Pd–Pd contributions were subtracted from the raw data with a difference file technique, the residual spectrum was expected to include only low-Z contributions that in this case appeared to be $Pd–O_{support}$ ones. However, an overall fit with a sum of $Pd–O_s$ and Pd–Pd contributions was not satisfactory until a second $Pd–O_l$ contribution at a longer distance was included. The optimized structural parameters determined from this fitting routine are summarized in Table 1 and the comparison of the overall fit with the raw EXAFS data is shown in Fig. 2A and B. The residual spectrum illustrating the Pd–Pd contributions in the $Pd^{n+}/Ce^{n+}/Na^{+}/\gamma\text{-}Al_2O_3$ sample after reduction with H_2 at

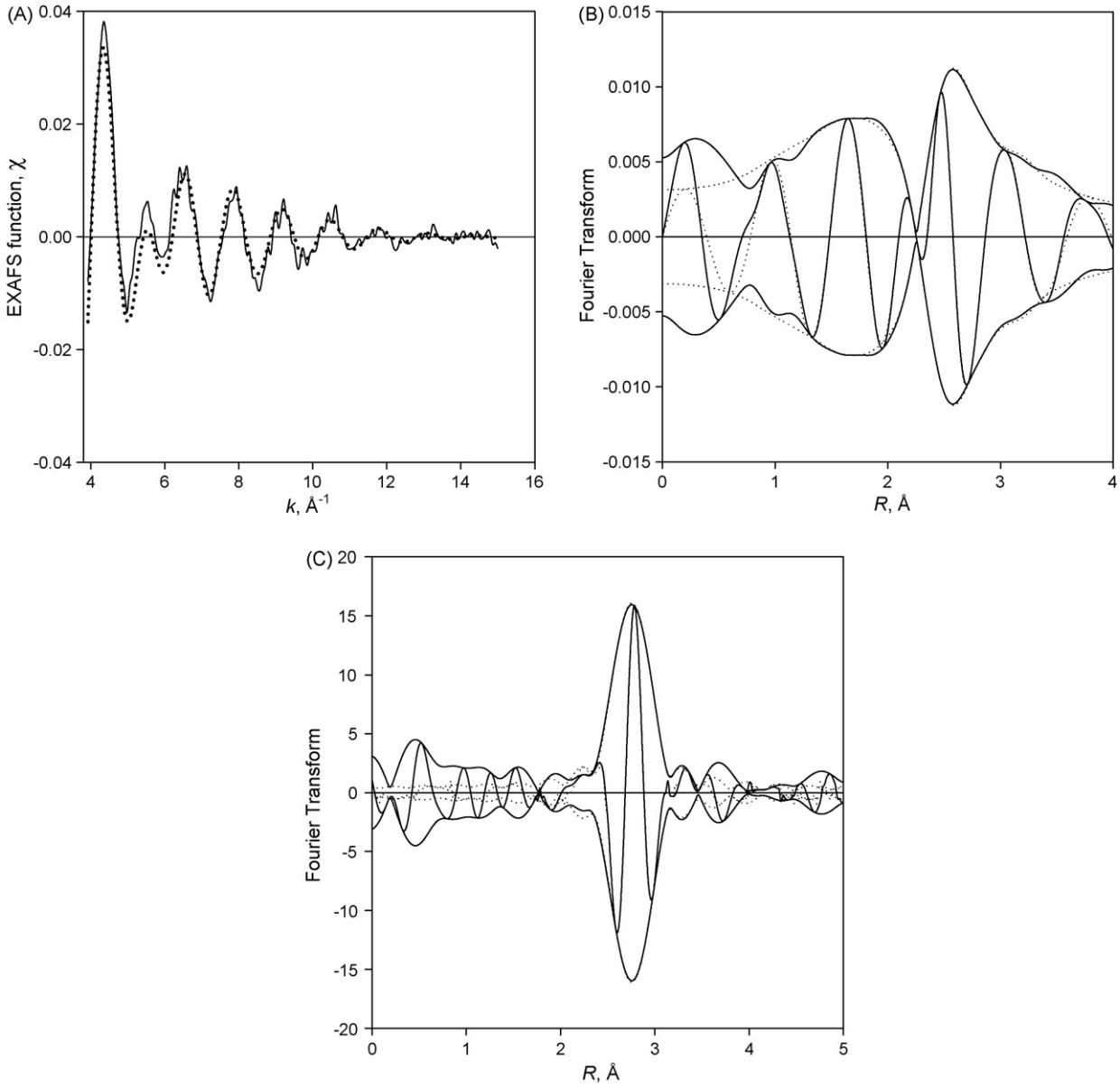

Fig. 2. (A) Experimental EXAFS (solid line) and sum of the calculated Pd–Pd + Pd–$O_{support}$ contributions (dotted line) characterizing a $Pd^{n+}/Ce^{n+}/Na^{+}/\gamma$-$Al_2O_3$ sample treated in H_2 at 500 °C. (B) Imaginary part and magnitude of uncorrected Fourier transform (k^0 weighted) of experimental EXAFS (solid line) and sum of the calculated Pd–Pd + Pd–$O_{support}$ contributions (dotted line) characterizing a $Pd^{n+}/Ce^{n+}/Na^{+}/\gamma$-$Al_2O_3$ sample after reduction with H_2 at 500 °C. (C) Residual spectrum illustrating the Pd–Pd contributions in the spectrum of a $Pd^{n+}/Ce^{n+}/Na^{+}/\gamma$-$Al_2O_3$ sample after reduction with H_2 at 500 °C: imaginary part and magnitude of phase- and amplitude-corrected Fourier transform (k^3 weighted) of experimental EXAFS minus calculated Pd–$O_{support}$ contributions (solid line) and calculated Pd–Pd contribution (dotted line).

500 °C is shown in Fig. 2C. Finally, only noise was left in the residual spectrum when all the contributions mentioned above were accounted for and subtracted from the raw data, indicating that no other contributions have to be included in the fit.

The optimized parameters summarized in Table 1 clearly indicate that in the reduced $Pd^{n+}/Ce^{n+}/Na^{+}/\gamma$-$Al_2O_3$ sample each Pd atom has on average approximately five near Pd neighbors at a bond distance of 2.76 Å. Such a small first-shell Pd–Pd coordination number allows us to conclude that only very small Pd clusters are present in the reduced sample, which is consistent with the weak oscillations observed in the high-k region, and the complete absence of higher Pd–Pd shells in the raw data. The data of Table 1 also show that each Pd atom interacts on average with approximately one oxygen atom at a distance of 2.10 Å and with one oxygen atom at a longer distance of 2.61 Å. Both of these contributions represent interactions of Pd atoms with the support. The shorter distance (2.10 Å) signifies the bonding between Pd atoms and oxygen anions of the support and has always been observed during EXAFS characterization of metals supported on various metal oxides and zeolites [31]. Longer metal-oxygen interactions (i.e., at distances between 2.5 and 2.7 Å) are also routinely observed in metal catalysts supported on metal oxide supports [31]. However, the exact origin of these longer Pd–$O_{support}$

contributions still remains under debate in the literature. Possible explanations include the presence of hydrogen atoms at the metal-support interface [32], or alternatively, weak metal-support interactions affected by cluster and support geometry [33,34].

In summary, the EXAFS data clearly indicate that freshly prepared $Pd^{n+}/Ce^{n+}/Na^{+}/\gamma\text{-}Al_2O_3$ incorporates Pd in a cationic form, likely as a highly dispersed palladium oxide species with Pd atoms largely isolated from each other. The reduction of such species in H_2 at temperatures as high as 500 °C leads to the formation of highly dispersed Pd clusters.

3.2. Interaction of NO with the various components of $Pd^{n+}/Ce^{n+}/Na^{+}/\gamma\text{-}Al_2O_3$

Since the $Pd^{n+}/Ce^{n+}/Na^{+}/\gamma\text{-}Al_2O_3$ material used has a complex chemical composition, each component of this sample was examined separately by in situ FTIR spectroscopy to determine its role in the adsorption of NO.

3.2.1. Interaction of NO with $\gamma\text{-}Al_2O_3$

When bare $\gamma\text{-}Al_2O_3$ was exposed to 500 ppm of NO in He at 300 °C (Fig. 3), four bands appeared in the FTIR spectrum at 1629, 1539, 1311 and 1230 cm^{-1}, indicating the formation of various nitrate/nitrite species [35]. The exact nature of these nitrates and nitrites cannot be unambiguously determined since some of their characteristic bands overlap. A complete assignment can only be achieved following a proper deconvolution of the spectra, which, however, is beyond the scope of this paper. The process of nitrate/nitrite formation was accompanied by a decrease in the concentration of isolated OH groups (characteristic band at 3762 cm^{-1}) and the appearance of a new band at 3547 cm^{-1} (Fig. 4), indicating that alumina hydroxyls actively participate in the surface chemistry. The

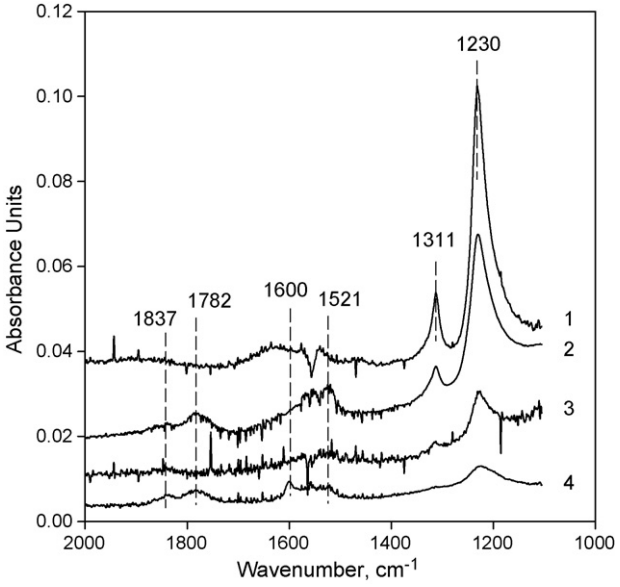

Fig. 3. FTIR spectra collected during exposure of: (1) $\gamma\text{-}Al_2O_3$ at 300 °C, (2) $Pd^{+}/\gamma\text{-}Al_2O_3$ at 300 °C, (3) $\gamma\text{-}Al_2O_3$ at 400 °C and (4) $Pd^{+}/\gamma\text{-}Al_2O_3$ at 400 °C to a 0.05% NO/He mixture.

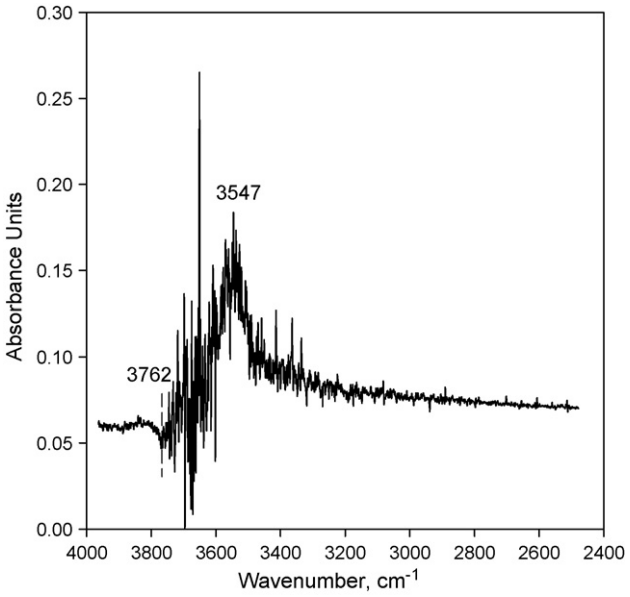

Fig. 4. FTIR spectrum of the OH region collected during exposure of $\gamma\text{-}Al_2O_3$ to a 0.05% NO/He mixture at 300 °C.

observed changes in the ν_{OH} region could be simply explained by the formation of hydrogen bonding between new adsorbates and the surface OH groups. However, no such interactions are expected with the various nitrite/nitrate species formed on the $\gamma\text{-}Al_2O_3$ surface. Alternatively, we may consider the possibility that acidic OH groups react with NO to form H_2O and NO^{+} species (the later would have a characteristic band at 2133 cm^{-1}), as it has been suggested previously [36]. However, no contribution from any such NO^{+} species was detected in our infrared spectra. It is also possible, however, that any NO^{+} species formed under our experimental conditions would react quickly with traces of water on the alumina surface to form nitrous acid [37].

$$NO + H_2O \rightarrow HNO_2 + H^{+} \quad (1)$$

Similarly, if any NO_2 species were to be produced by NO oxidation or NO disproportionation, they would undergo further transformations on a surface containing traces of water to form nitrous and nitric acids [38].

$$NO_2 + NO + H_2O \rightarrow 2HNO_2 \quad (2)$$

$$2NO_2 + H_2O \rightarrow HNO_2 + HNO_3 \quad (3)$$

In fact, the formation of HNO_3 species due to the interaction of NO_2 with a SiO_2 surface has been previously confirmed by FTIR [38]. Since no other species besides NO (characteristic bands at 1907 and 1845 cm^{-1}) were detected in the gas phase during our experiments, we may infer that all species formed during exposure of $\gamma\text{-}Al_2O_3$ to NO remained adsorbed on the surface. The coverage of the $\gamma\text{-}Al_2O_3$ surface by hydroxyls in the 300–400 °C temperature range is expected to be rather high. Therefore, it is conceivable that the reactions mentioned above can also proceed at these elevated temperatures with the participation of the surface hydroxyl groups, resulting in the formation of various surface HNO_x species. Both HNO_2 and

HNO_3 have characteristic OH stretching vibrations in the 3500–3572 cm^{-1} region [38,39] and therefore, the appearance of the band at 3547 cm^{-1} is consistent with the formation of such surface species under our experimental conditions.

Alternatively, it is also possible that NO molecules can coordinate to the surface hydroxyl groups according to the following reaction:

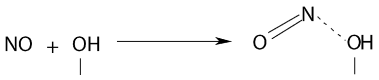

(4)

If such coordination were to take place, it would lead to the formation of an HONO type species. In such a case, the band at approximately 3547 cm^{-1}could be the result of a shift of the ν_{OH} mode (3762 cm^{-1}) to a lower frequency region, which is typical for HNO_x type compounds [38,39].

3.2.2. Interaction of NO with Na^+/γ-Al_2O_3

When γ-Al_2O_3 was modified by Na^+ cations and exposed to 500 ppm of NO in He at 300 °C, bands at 1568, 1372, 1312 and 1225 cm^{-1} (Fig. 5) appeared in the FTIR specta. Identical spectra were obtained when the temperature was further increased to 400 °C. Similar to the case of bare γ-Al_2O_3, the bands at 1568, 1312, and 1225 cm^{-1} can be assigned to nitrate/nitrite species formed on the γ-Al_2O_3 surface. The concentration of these species is somewhat higher than that on bare γ-Al_2O_3, which suggests that sodium promotes to some degree the formation of such nitrite/nitrate species.

A comparison of the infrared data summarized in Figs. 3 and 5 clearly points out that the band at 1372 cm^{-1} is a "signature" band indicating the presence of a new type of NO_x surface species that was absent from the bare γ-Al_2O_3 surface. As shown previously, both NaOH and Na_2O can interact with NO and form nitrite/nitrate species [40,41]. Since in our case, sodium is present on the catalyst surface, most likely in an oxidized form, we suggest that the exposure of the sample to NO leads to the formation of NO_2^-/NO_3^- species associated with sodium cations. It has been reported previously that NO_2^- species associated with Na^+ ions in NaY zeolites show characteristic infrared bands at approximately 1275 cm^{-1}, while NO_3^- ions have infrared features in the 1300–1500 cm^{-1} region [37,42]. Moreover, sodium nitrate has five infrared active internal vibrational modes with corresponding bands at 1789, 1447, 1378, 836 and 726 cm^{-1} [43]. Only the most intense bands at 1378 and 836 cm^{-1} are prominent in infrared spectra at elevated temperatures. Therefore, the band at 1372 cm^{-1} observed in the spectrum of Na^+/γ-Al_2O_3 after exposure to NO at 300–400 °C can be confidently assigned to a sodium nitrate species. Apparently, the other expected band at approximately 840 cm^{-1} cannot be observed due to the overlap with the vibration of the alumina. From this point of view, our data are consistent with a previous literature report according to which the formation of sodium nitrates results to a single characteristic band observed at 1390 cm^{-1} when a sodium form of mordenite was exposed to NO and O_2 [44]. Furthermore, the formation of both $NaNO_2$ and $NaNO_3$ species has been confirmed by XPS following exposure of $Pt/Na/Al_2O_3$ samples to a NO/C_3H_6 mixture [45].

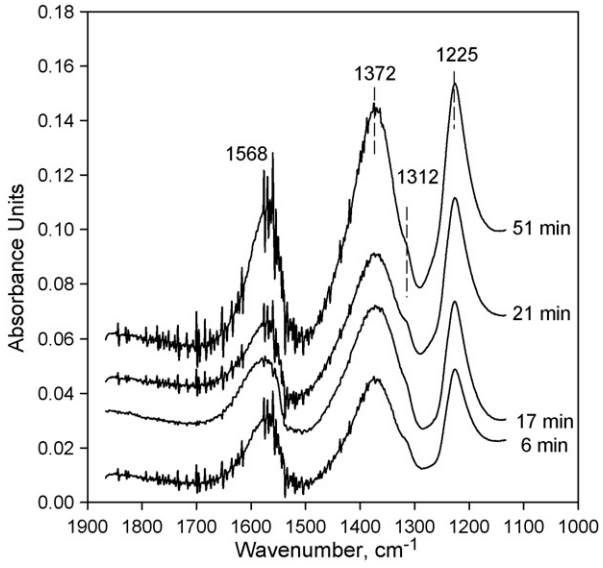

Fig. 5. FTIR spectra collected at different times during exposure of Na^+/γ-Al_2O_3 to a 0.05% NO/He mixture at 300 °C.

Finally, it is also interesting to note that upon exposure of Na^+/γ-Al_2O_3 to NO, the changes observed in the OH region completely reproduce those observed for the bare γ-Al_2O_3, indicating that the presence of the Na^+ cations does not affect substantially this component of the γ-Al_2O_3 surface chemistry. Any HNO_x type species formed on the surface would be also expected to interact with sodium to form $NaNO_x$. H^+ generated as a result of this process would further coordinate to OH groups, leading to the appearance of characteristic ν_{OH} vibrations of bridging OH groups in the low frequency region [42].

3.2.3. Interaction of NO with Pd^{n+}/γ-Al_2O_3

When a freshly prepared Pd^{n+}/γ-Al_2O_3 sample was exposed to 500 ppm of NO in He at the 300–400 °C temperature range, in addition to the nitrate/nitrite species formed on γ-Al_2O_3, two new low intensity bands were observed at 1837 and 1782 cm^{-1} (Fig. 3), which can be assigned to NO adsorbed on the Pd^{n+} cations [35,46,47]. The absence of any bands characteristic of terminal nitrosyl (at 1730–1750 cm^{-1}), bent NO (at 1650–1670 cm^{-1}) or bridged-bonded NO (at 1570 cm^{-1}) species that are typically observed following the adsorption of NO on metallic Pd [48], clearly indicates that palladium is present in the sample in a cationic form, consistent with the EXAFS results discussed above.

The presence of Pd cations on the γ-Al_2O_3 surface does not substantially affect the formation of nitrate/nitrite species in the 300–400 °C temperature range, as evidenced by the presence of the bands in the 1600–1230 cm^{-1} range. However, in the presence of Pd^{n+}, the intensity of the bands at 1311 and 1230 visibly declined, while the intensity of the bands at 1600 and 1521 cm^{-1} slightly increased as compared to the intensities of the same bands observed with bare γ-Al_2O_3 (Fig. 3). Although these changes are not very dramatic, they indicate a decreasing concentration of nitrites and a corresponding increasing

concentration of nitrates on the γ-Al_2O_3 surface in the presence of Pd, suggesting that the PdO species facilitate either the process of NO oxidation, or its dissociation leading to the spillover of oxygen on the support where it can facilitate the formation of nitrates. Additional experiments performed with this sample indicate that the bands at 1837 and 1782 cm^{-1} can be completely removed by the addition of oxygen to the NO flow, which suggests that the NO species adsorbed on Pd^{n+} cations are highly reactive.

3.2.4. Interaction of NO with Ce^{n+}/γ-Al_2O_3

The addition of ceria to γ-Al_2O_3 did not lead to any dramatic changes in the FTIR spectra collected, indicating a minimal effect of ceria on the NO adsorption process (Fig. 6). Once again, the bands observed at 1551, 1524, 1312 and 1231 cm^{-1} can be assigned to various types of nitrite/nitrate species. However, their location remains uncertain because such species have similar absorption bands whether they are formed on γ-Al_2O_3 or CeO_2. For example, the band at 1551 cm^{-1} could be assigned to nitrates adsorbed on γ-Al_2O_3 or to NO_2^-/NO_3^- species formed on CeO_2 [49]. Moreover, nitrosyl complexes coordinated on Ce^{n+} cations associated with oxygen defects also exhibit a characteristic band at 1550 cm^{-1} [49]. Therefore, from the data of Fig. 6 alone, it is difficult to determine whether or not some of these species were formed on ceria. Also, some previous literature reports indicate that the adsorption of NO on CeO_2 is very slow [49].

Nevertheless, it is noteworthy to point out that the bands at 1312 and 1231 cm^{-1} appeared to be less intense, while the bands at 1551 and 1524 cm^{-1} are much stronger on the ceria modified alumina as compared to the similar bands on bare γ-Al_2O_3. If we assume that bands in the 1500 cm^{-1} region represent mainly nitrates and those at lower wavenumbers (1200–1312 cm^{-1}) mainly nitrites, we can conclude that the presence of ceria promotes the formation of nitrates at the expense of nitrites. Such an effect could be associated with the ability of ceria to store and provide oxygen [50]. This key feature is attributed to the ability of ceria to release its lattice oxygen with ease and form oxygen vacancies with adjacent Ce^{4+} cations being reduced to Ce^{3+} [51,52]. Literature reports indicate that to some degree, oxygen vacancies may be generated on ceria surfaces directly by NO adsorption [49], implying that nitrite/nitrate species could be formed directly on ceria without any additional source of oxygen. Such a process appears to be consistent with our infrared data (Fig. 6).

In this case, similar to the bare Al_2O_3, the population of surface species was substantially decreased as the temperature was increased from 300 to 400 °C (Fig. 6), indicating that the thermal stability of the adsorbed surface species was not affected by the presence of ceria.

3.2.5. Interaction of NO with Ce^{n+}/Na^+/γ-Al_2O_3

When a sample containing both Na^+ and Ce^{n+} was exposed to 500 ppm NO in He at 300 °C, the FTIR spectra obtained (Fig. 7) contained all the bands previously observed in the individual spectra of the Ce^{n+}/γ-Al_2O_3 and Na^+/γ-Al_2O_3 samples. The bands at 1574, 1312 and 1229 cm^{-1}, for example, are characteristic of nitrate/nitrite species formed on the γ-Al_2O_3 and/or CeO_2 surfaces, while the band at 1372 cm^{-1} is clearly related to nitrate species associated with Na^+. The concentration of nitrate/nitrite species in this sample is apparently higher than that on pure γ-Al_2O_3, which is consistent with our earlier conclusions that both sodium and ceria promote the formation of nitrites/nitrates. However, sodium appears to dominate the surface chemistry, since the intensities of the bands in the spectra obtained for the Ce^{n+}/Na^+/γ-Al_2O_3 sample are similar to those in the Na^+/γ-Al_2O_3 material.

When the exposure to NO was conducted with a fresh sample at 400 °C, the intensity of the band at 1574 cm^{-1}

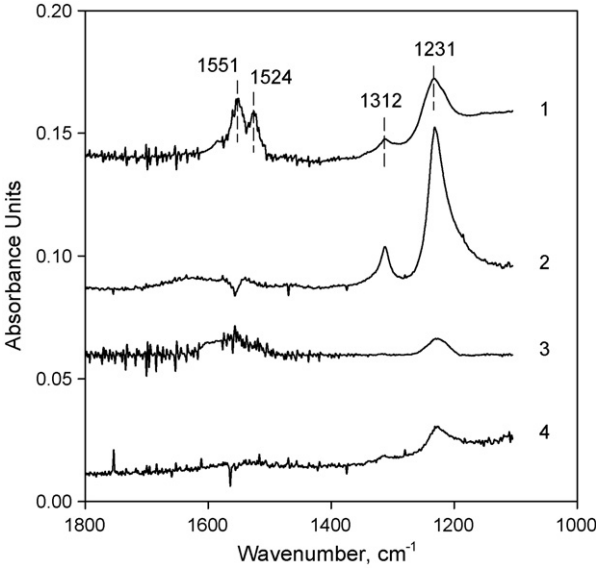

Fig. 6. FTIR spectra collected during exposure of Ce^{n+}/γ-Al_2O_3 to a 0.05% NO/He mixture at: (1) 300 °C and (3) 400 °C. FTIR spectra collected during exposure of γ-Al_2O_3 to a 0.05% No/He mixture at: (2) 300 °C and (4) 400 °C.

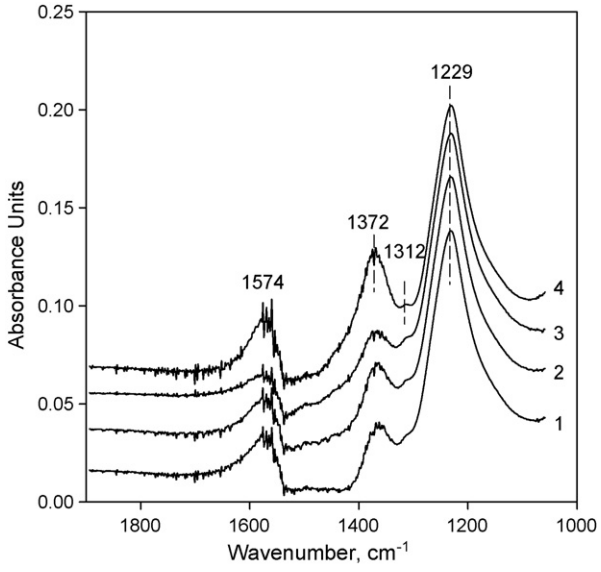

Fig. 7. FTIR spectra collected during exposure of a Ce^{n+}/Na^+/γ-Al_2O_3 sample to a 0.05% NO/He mixture at 300 °C for: (1) 2 min, (2) 23 min, (3) 60 min and (4) 80 min.

previously assigned to surface nitrates remained approximately the same, while the bands at 1372, 1312 and 1229 cm^{-1} declined in intensity, indicating that surface nitrates are more stable at elevated temperatures than either the nitrites and/or the nitrate species associated with Na^+, consistent with earlier literature reports illustrating that the thermal stability of nitrates is higher than nitrites on various surfaces [42,45]. It is interesting to note, that the band at 3547 cm^{-1} observed in the hydroxyl region was much stronger at 300 °C than at 400 °C (data not shown for brevity), suggesting that this band and the bands at 1312 and 1229 cm^{-1}may represent the same surface species, the concentration of which declines with temperature.

3.2.6. Interaction of NO with $Pd^{n+}/Ce^{n+}/Na^+/\gamma$-$Al_2O_3$

In general, the addition of Pd^{n+} does not change the type and distribution of surface species formed on the $Ce^{n+}/Na^+/\gamma$-Al_2O_3 surface after exposure to NO in the 300–400 °C temperature range; the spectra observed were identical to those reported in Fig. 7 for the $Ce^{n+}/Na^+/\gamma$-Al_2O_3 sample. However, the two low intensity bands at 1837 and 1782 cm^{-1}, previously assigned to NO species adsorbed on Pd^{n+} cations in the spectra of the Pd^{n+}/γ-Al_2O_3 (Fig. 3), were not detected in the spectra of the $Pd^{n+}/Ce^{n+}/Na^+/\gamma$-$Al_2O_3$ sample, indicating that either the chemisorptive properties of Pd^{n+} were greatly reduced in the presence of the sodium and ceria additives, or that the Pd^{n+} sites were blocked by these additives. Alternatively, it is also possible that NO species adsorbed on Pd^{n+} at 300–400 °C in the presence of the sodium and ceria additives become very active and have a short life time prior to migrating in the form of nitrites/nitrates to the other sample components. Such a suggestion is also consistent with the previous observation regarding the role of PdO as facilitators of nitrate/nitrite formation on the γ-Al_2O_3 surface (Fig. 3).

3.3. Interaction of a NO/O_2 mixture with the various components of $Pd^{n+}/Ce^{n+}/Na^+/\gamma$-$Al_2O_3$

3.3.1. Interaction of NO/O_2 with γ-Al_2O_3

When γ-Al_2O_3 was exposed to a 0.05% NO/1% O_2/He mixture, the concentration of nitrate/nitrite species formed was substantially increased (Fig. 8, spectrum 1). Regardless of the temperature used, this process was accompanied by evolution of gas phase NO_2 (characteristic infrared bands at 1627 and 1589 cm^{-1}) indicating extensive oxidation of NO by O_2 at these conditions. The nitrate/nitrite species formed on the γ-Al_2O_3 surface were stable and their concentration on the surface remained unchanged following treatment with He at either 300 or 400 °C. Assuming that nitrites are precursors of nitrates, it is expected that when the NO/O_2/He flow is replaced by O_2/He the nitrate species will dominate the γ-Al_2O_3 surface. Thus, the bands observed at 1583, 1552 and 1243 cm^{-1} (Fig. 8, spectra 2–3) can be assigned to different types of surface nitrate species. Furthermore, the difference spectrum (Fig. 8, spectrum 4) obtained from the spectra collected under NO/O_2/He and O_2/He flows demonstrates the transformation from the nitrite to the nitrate species. Since no desorption of either nitrite or nitrate species was observed under He flow, negative bands observed at

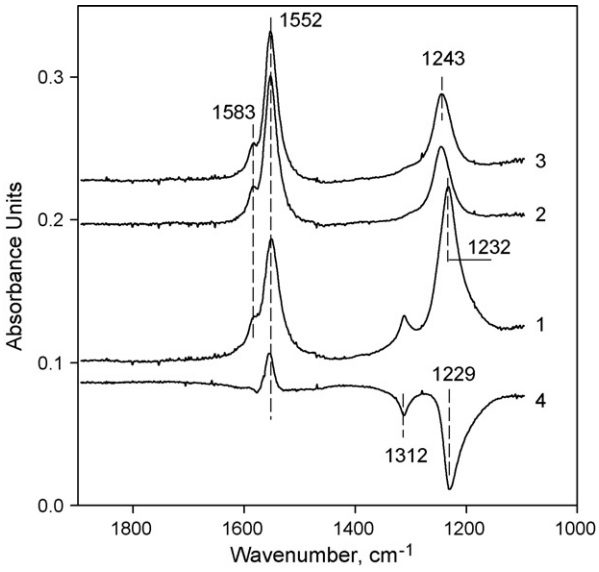

Fig. 8. FTIR spectra collected during exposure of γ-Al_2O_3 to: (1) a 0.05% NO/1% O_2/He mixture at 300 °C and subsequent exposure to a 1% O_2/He mixture for (2) 13 min, and (3) 60 min at 300 °C. Spectrum 4 is the difference between spectra 3 and 1.

1312 and 1229 cm^{-1} in this difference spectrum are associated with species disappearing under O_2/He flow and therefore could be assigned to the nitrite species. Based on these assignments, we can conclude that when γ-Al_2O_3 is exposed only to NO, nitrites are predominantly formed on the surface due to the lack of sufficient O_2 for their conversion to nitrates. However, when additional O_2 is present, the surface is covered by both nitrites and nitrates. In this case, the band observed at 1232 cm^{-1} (Fig. 8) is most likely a combination band that is formed by the overlapping of the 1243 cm^{-1} band of nitrates with the 1229 cm^{-1} band of nitrites.

3.3.2. Interaction of NO/O_2 with Pd^{n+}/γ-Al_2O_3

When Pd cations were present on the γ-Al_2O_3 surface, the addition of O_2 to the NO/He flow in the 300–400 °C temperature range resulted in a substantial increase of the concentration of nitrates/nitrites with the former dominating on the surface, suggesting that Pd^{n+} cations promote the transformation of NO to surface nitrates/nitrites. Similar to the case of bare γ-Al_2O_3, NO_2 was once again detected in the gas phase, indicating that not all the NO oxidized on Pd^{n+} remained adsorbed on the support.

3.3.3. Interaction of NO/O_2 with Na^+/γ-Al_2O_3

No significant differences were observed in the intensities of the bands at 1570, 1312 and 1229 cm^{-1} associated with nitrite/nitrate species in the spectra of a Na^+/γ-Al_2O_3 sample exposed to NO in the presence and absence of O_2 (Fig. 9, spectra 1 and 2). This behavior is different from what was observed with bare γ-Al_2O_3 and Pd^{n+}/γ-Al_2O_3 (Fig. 8), suggesting that nearly a maximum surface concentration of nitrates/nitrites can already be attained after exposure of the Na^+/Al_2O_3 sample to NO in the absence of O_2. We can further suggest that the role of sodium in these samples may not be limited to direct interactions with NO

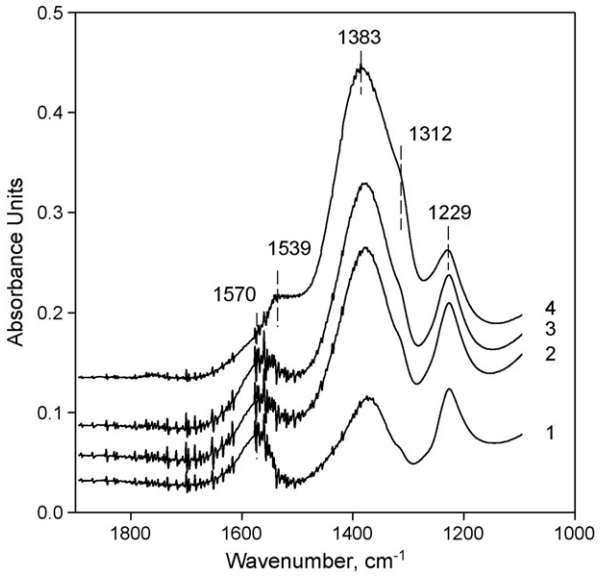

Fig. 9. FTIR spectra collected during exposure of a $Na^+/\gamma\text{-}Al_2O_3$ sample to (1) a 0.05% NO/He mixture for 90 min at 300 °C and subsequent exposure to (2) a 0.05% NO/0.2% O_2/He mixture for 70 min and a 0.05% NO/1% O_2/He mixture for (3) 10 min and (4) 90 min at 300 °C.

leading to the formation of various nitrite/nitrate species associated with sodium, as we have pointed out in Section 3.2.2. Another possible mechanism that can be used to rationalize the role of Na^+ involves the decomposition of NO leading to the formation of N_2O and oxygen. Oxygen species thus formed can subsequently react with NO to form nitrites/nitrates. Literature reports indeed indicate that the decomposition of NO can proceed on oxide surfaces [53]. Since under our experimental conditions we did not observe any characteristic absorption bands associated with N_2O (two such bands are known at 2230–2270 and 1250–1320 cm^{-1}) either in the gas phase or on the surface, it is suggested that if any such species was formed, it rapidly underwent subsequent decomposition at these elevated temperatures to yield nitrogen and oxygen:

$$2N_2O \rightarrow 2N_2 + O_2 \quad (5)$$

One difference that was observed in the spectra of $Na^+/\gamma\text{-}Al_2O_3$ collected in the presence and absence of O_2 was related to the intensity of the band observed at 1372 cm^{-1} and assigned to the sodium nitrate species (Fig. 5). This band increased substantially in intensity, shifted to 1383 cm^{-1} (Fig. 9), and became the most dominant one in the spectrum. These results suggest that under oxidizing conditions NO_3^- species dominate the $Na^+/\gamma\text{-}Al_2O_3$ surface and are most likely associated with Na^+ cations rather than with the $\gamma\text{-}Al_2O_3$ surface. Moreover, under similar conditions, the exposure of $\gamma\text{-}Al_2O_3$ to the NO/O_2 mixture led to the formation of NO_2 in the gas phase. In the case of the $Na^+/\gamma\text{-}Al_2O_3$ sample, there were no indications of any NO_2 formation in the gas phase at 300 °C, suggesting that all nitrite/nitrate species formed remained on the surface. This further suggests that the role of Na^+ cations is to trap the NO_x species formed and retain them on the surface (most likely in the form of $NaNO_3$).

When the temperature was increased to 400 °C, the band at 1383 cm^{-1} still remained the most intense among the other nitrate/nitrite bands in the spectrum, suggesting that nitrate species associated with Na^+ continue to dominate the surface even at these temperatures. However, trace amounts of gaseous NO_2 were detectable at this temperature, suggesting the onset of nitrate/nitrite decomposition, although, it is not possible to establish whether the decomposing NO_x species were associated with alumina or Na^+.

3.3.4. Interaction of NO/O_2 with $Ce^{n+}/\gamma\text{-}Al_2O_3$

Similar to what was observed with previous samples, when O_2 was added to the NO feed, the intensity of all bands was substantially increased in the specta of $Ce^{n+}/\gamma\text{-}Al_2O_3$, indicating that nitrates once again dominate the surface under these conditions (Fig. 10). Furthermore, the stronger intensities of the absorption bands observed for $Ce^{n+}/\gamma\text{-}Al_2O_3$ (Fig. 10), as compared to those observed on bare $\gamma\text{-}Al_2O_3$ under similar conditions (Fig. 8), suggest that ceria also promotes the formation of nitrates under oxidizing conditions. Similar to what was observed with the $Na^+/\gamma\text{-}Al_2O_3$ sample, the NO_x species formed remained trapped on the surface and no indication of gaseous product formation was observed at temperatures up to 400 °C, while over bare $\gamma\text{-}Al_2O_3$ gas phase NO_2 was observed even at 300 °C.

3.3.5. Interaction of NO/O_2 with $Pd^{n+}/Ce^{n+}/Na^+/\gamma\text{-}Al_2O_3$

The addition of 0.2% O_2 to the 0.05% NO/He mixture at 300 °C led to a substantial increase in the concentration of the surface nitrate/nitrite species formed over the $Pd^{n+}/Ce^{n+}/Na^+/\gamma\text{-}Al_2O_3$ sample (Fig. 11). Under these conditions the intensities of the bands at 1543, 1384, 1317 and 1246 cm^{-1} (assigned to

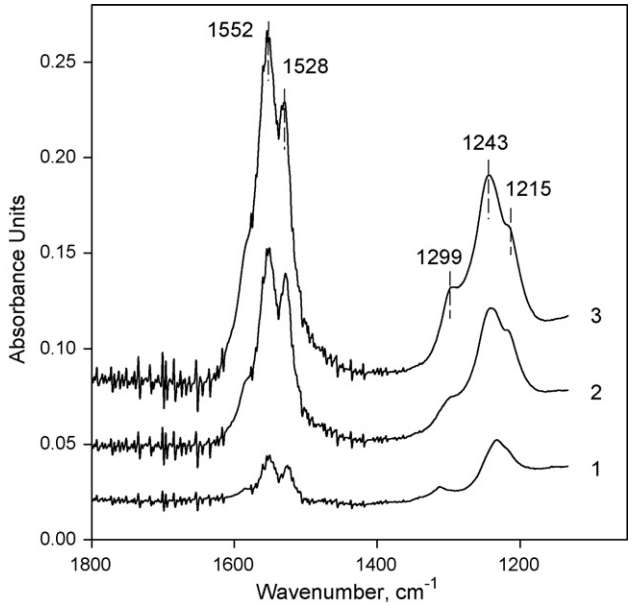

Fig. 10. FTIR spectra collected during exposure of a $Ce^{n+}/\gamma\text{-}Al_2O_3$ sample to (1) a 0.05% NO/He mixture for 60 min at 300 °C and subsequent exposure to (2) a 0.05% NO/0.2% O_2/He mixture for 60 min and (3) 0.05% NO/1% O_2/He mixture for 60 min at 300 °C.

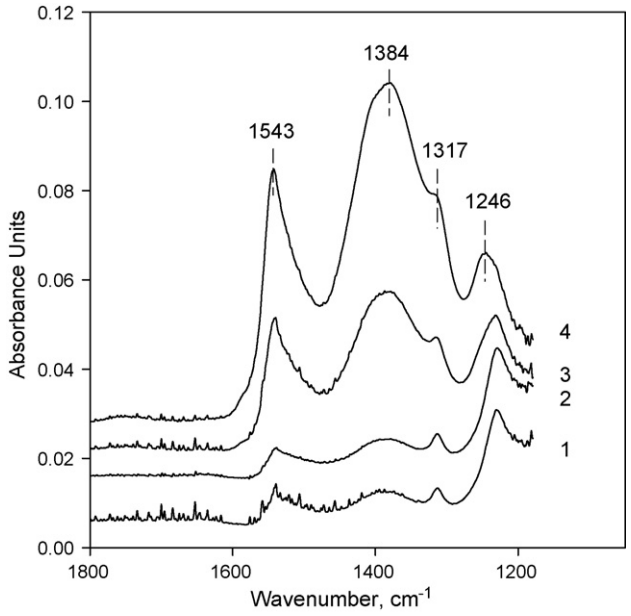

Fig. 11. FTIR spectra collected during exposure of a $Pd^{n+}/Ce^{n+}/Na^{+}/\gamma\text{-}Al_2O_3$ sample to: (1) a 0.05% NO/He mixture for 60 min at 300 °C and subsequent exposure to a 0.05% NO/0.2% O_2/He mixture for (2) 5 min, and (3) 60 min and (4) 0.05% NO/1% O_2/He mixture for 60 min at 300 °C.

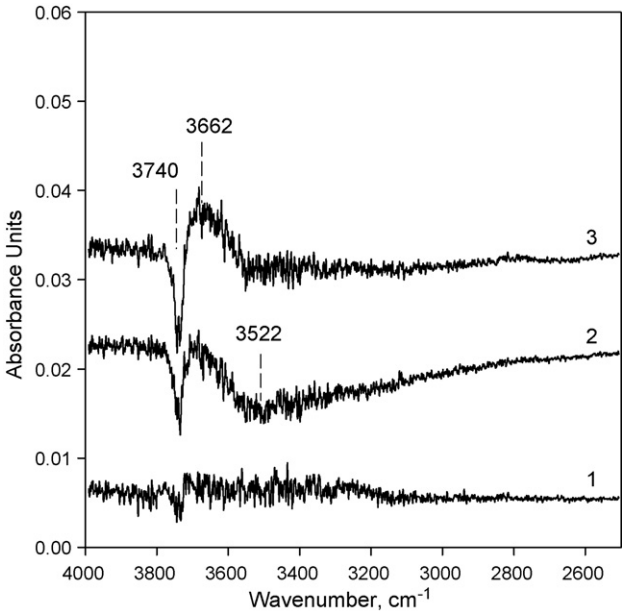

Fig. 12. FTIR difference spectra illustrating changes in the ν_{OH} region during treatment of a $Pd^{n+}/Ce^{n+}/Na^{+}/\gamma\text{-}Al_2O_3$ sample that had been exposed to a 0.05% NO/He mixture at the following conditions: in a 0.05% NO/0.2% O_2/He mixture at 300 °C for: (1) 5 min and (2) 60 min; (3) in a 0.05% NO/1% O_2/He mixture at 300 °C for 60 min.

various nitrate/nitrite species) continued to increase substantially with time on stream (Fig. 11, spectra 2 and 3). A further increase in the concentration of O_2 to 1% led to another increase in the intensities of the nitrite/nitrate bands, which clearly indicates that gas phase O_2 promotes the formation of the nitrite/nitrate species while the surface is not saturated. All nitrite/nitrate species formed remained trapped on the surface. Similar to the case of $Na^{+}/\gamma\text{-}Al_2O_3$, the spectra of Fig. 11 also indicate that sodium dominates the surface chemistry in the $Pd^{n+}/Ce^{n+}/Na^{+}/\gamma\text{-}Al_2O_3$ sample, since the nitrate species associated with sodium (characteristic band at 1384 cm^{-1}) appear to have the highest concentration.

Similar results were obtained when the temperature was increased to 400 °C (data not shown for brevity). The nitrate/nitrite species associated with the $Ce^{n+}/\gamma\text{-}Al_2O_3$ component of the support (characteristic bands at 1543, 1317 and 1246 cm^{-1}) were not substantially affected by the temperature increase. However, the concentration of nitrate species associated with sodium (characteristic band at 1384 cm^{-1}) appeared to be reduced by half. This result can be attributed either to a low thermal stability of the sodium nitrate species, or to a decreased concentration of the necessary precursors for the formation of such species at elevated temperatures. For example, the formation of sodium nitrate may not be the result of a direct reaction between the Na^{+} cations and NO, but it may first require the adsorption of gas phase NO on surface hydroxyls, followed by the reaction of the HNO_x surface species formed with Na^{+}. In this case, the amount of nitrate species accumulated on sodium would depend on the concentration of hydroxyls that in turn, is a function of temperature.

In general, the surface chemistry taking place when $Pd^{n+}/Ce^{n+}/Na^{+}/\gamma\text{-}Al_2O_3$ is exposed to the NO/O_2 mixture at elevated temperatures appears to be fairly complex and involves surface hydroxyls, as indicated by changes observed in the 3400–3800 cm^{-1} region. For example, when 0.2% O_2 was added to the NO flow at 300 °C, the intensity of the band characteristic of isolated OH groups at 3740 cm^{-1} decreased with time on stream (Fig. 12, spectrum 2). This process was also accompanied by a decrease in the intensity of the band at 3522 cm^{-1}, indicating that the HNO_x species formed when the sample was already exposed to NO underwent further transformation. Moreover, when the concentration of O_2 was further increased to 1%, the decrease in the concentration of isolated OH groups (band at 3740 cm^{-1}) was also accompanied by the appearance of a new band at 3662 cm^{-1} (Fig. 12, spectrum 3), which can be assigned to the symmetric stretching vibration of H_2O. Therefore, the following tentative scheme can be proposed for the formation of surface species:

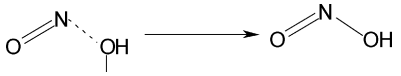

(6)

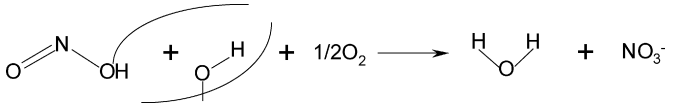

(7)

When the $Pd^{n+}/Ce^{n+}/Na^{+}/\gamma\text{-}Al_2O_3$ sample was exposed to NO in the absence of O_2, only the first reaction took place, leading to the formation of HNO_2-type species. These species can further react with hydroxyls in the presence of O_2 yielding H_2O and surface NO_3^{-} (reaction (7)) that remain trapped under

the conditions examined. The decomposition of HNO_x species is still observed at 400 °C, as indicated by the decrease in the intensity of the characteristic band at approximately 3500 cm^{-1} (spectra not shown). However, no accumulation of H_2O or decrease in the concentration of the isolated OH groups was detected. It is likely, that at this temperature the water formed does not remain on the surface and the process of regeneration of isolated OH groups is very fast and cannot be detected spectroscopically.

4. Conclusions

EXAFS results indicate that in a freshly prepared $Pd^{n+}/Ce^{n+}/Na^{+}/\gamma\text{-}Al_2O_3$ sample, similar to materials used commercially as FCC NO_x additives, palladium is present in the form of highly dispersed PdO species. The reduction of such species with H_2 at temperatures as high as 500 °C led to the formation of small and largely isolated Pd clusters in which each Pd atom has approximately five near Pd neighbors at a bond distance of 2.76 Å. All components of this material can interact with NO and promote the formation of surface nitrates/nitrites to various degrees, with the process being accelerated in the presence of oxygen. However, the presence of both Na^+ and Ce^{n+} does not only promote the formation of nitrates/nitrites, but also results in the trapping of the NO_x species formed on the surface of this material. Furthermore, Na^+ appears to dominate the surface chemistry and readily forms sodium nitrates upon exposure to NO. The rate of this process is further increased in the presence of O_2. Hydroxyls from the support also participate in the surface chemistry through the formation of a HNO_x-type precursor, which eventually decomposes to yield the surface nitrates.

Acknowledgements

The authors gratefully acknowledge W.R. Grace & Co.-Conn. for financial support and permission to publish this work. Use of the National Synchrotron Light Source, Brookhaven National Laboratory, was supported by the U.S. Department of Energy, Office of Science, Office of Basic Energy Sciences, under Contract No. DE-AC02-98CH10886. Portions of this research were also carried out at the Stanford Synchrotron Radiation Laboratory, a national user facility operated by Stanford University on behalf of the U.S. Department of Energy, Office of Basic Energy Sciences. We are grateful to the beamline staff at both facilities for their assistance.

References

[1] G.H. Unzelman, AM 88-25, Natl. Pet. Refiners Assoc. Annual Meeting, San Antonio, 1988.
[2] W.-C. Cheng, G. Kim, A.W. Peters, X. Zhao, K. Rajagopalan, M.S. Ziebarth, Catal. Rev. Sci. Eng. 40 (1998) 39.
[3] R.H. Harding, A.W. Peters, J.R.D. Nee, Appl. Catal. A 221 (2001) 389.
[4] X. Zhao, A.W. Peters, G.D. Weatherbee, Ind. Eng. Chem. Res. 36 (1997) 4535.
[5] A.W. Peters, G. Yaluris, G.D. Weatherbee, X. Zhao, Chem. Ind. 74 (1998) 259.
[6] G. Yaluris, T.J. S Dougan, AM 05-21 National Petroleum Refiners Association Annual Meeting, San Antonio, 2005.
[7] A.W. Peters, J.A. Rudesill, G.D. Weatherbee, E.F. Rakeiwicz, Barbato-Grauso, X. Zhao, US Patent 6,280,607 (2001) (to W.R.Grace & Co.-Conn.).
[8] A.W. Peters, J.A. Rudesill, G.D. Weatherbee, E.F. Rakeiwicz, Barbato-Grauso, US Patent 6,143,167 (2000) (to W.R.Grace & Co.-Conn.).
[9] A.W. Peters, E.F. Rakeiwicz, G.D. Weatherbee, X. Zhao, US Patent 6,165,933 (2000) (to W.R.Grace & Co.-Conn.).
[10] G. Yaluris, J.A. Rudesill, US Patent 6,881,390 (2005) (to W.R.Grace & Co.-Conn.).
[11] A. Corma, A.E. Palomares, F. Rey, F. Marquez, J. Catal. 170 (1997) 140.
[12] G. Yaluris, A.W. Peters, in: J.G. Reynolds, M.R. Khan (Eds.), Designing Transportation Fuels for a Cleaner Environment, Taylor & Francis, Philadelphia, 1999, pp. 151–164.
[13] J.-O. Barth, A. Jentys, J.A. Lercher, Ind. Eng. Chem. Res. 43 (2004) 3097.
[14] J.-O. Barth, A. Jentys, J.A. Lercher, Ind. Eng. Chem. Res. 43 (2004) 2368.
[15] I.V. Babich, K. Seshan, L. Lefferts, Appl. Catal. B 59 (2005) 205.
[16] E.F. Iliopoulou, E.A. Efthimiadis, L. Nalbandian, I.A. Vasalos, J.-O. Barth, J.A. Lercher, Appl. Catal. B: Environ. 60 (2005) 277.
[17] E.F. Iliopoulou, E.A. Efthimiadis, L. Nalbandian, I.A. Vasalos, J.-O. Barth, J.A. Lercher, Appl. Catal. B: Environ. 47 (2004) 165.
[18] O.S. Alexeev, S. Krishnamoorthy, C. Jensen, M.S. Ziebarth, G. Yaluris, T.G. Roberie, M.D. Amiridis, Top. Catal., in press.
[19] T. Chafik, O. Dulaurent, J.L. Gass, D. Bianchi, J. Catal. 179 (1998) 503.
[20] S. Kawi, O. Alexeev, M. Shelef, B.C. Gates, J. Phys. Chem. 99 (1995) 6926.
[21] M. Vaarkamp, J.C. Linders, D.C. Koningsberger, Physica B 208–209 (1995) 159.
[22] D.C. Koningsberger, in: C.A. Melendres, A. Tadjeddine (Eds.), Synchrotron Techniques in Interfacial Electrochemistry, Kluwer, Dordrecht, 1994, p. 181.
[23] E.A. Stern, Phys. Rev. B 48 (1993) 9825.
[24] E.O. Brigham, The Fast Fourier Transform, Prentice-Hall, Englewood Cliffs, NJ, 1974.
[25] P.S. Kirlin, F.B.M. van Zon, D.C. Koningsberger, B.C. Gates, J. Phys. Chem. 94 (1990) 8439.
[26] J.B.A.D. van Zon, D.C. Koningsberger, H.F.J. van't Blik, D.E. Sayers, J. Chem. Phys. 82 (1985) 5742.
[27] M. Vaarkamp, Ph.D. Thesis, Eindhoven University, The Netherlands, 1993.
[28] F.W. Lytle, D.E. Sayers, E.A. Stern, Physica B 158 (1988) 701.
[29] D.C. Koningsberger, B.L. Mojet, G.E. van Dorssen, D.E. Ramaker, Top. Catal. 10 (2000) 143.
[30] R.W.G. Wyckoff, Crystal Structures Interscience, vol. 1, John Wiley & Sons, 1963.
[31] O. Alexeev, B.C. Gates, Top. Catal. 10 (2000) 273.
[32] M. Vaarkamp, F.S. Modica, J.T. Miller, D.C. Koningsberger, J. Catal. 144 (1993) 611.
[33] S.E. Deutsch, G. Mestl, H. Knözinger, B.C. Gates, J. Phys. Chem. B 101 (1997) 1374.
[34] A.M. Ferrari, K.M. Neyman, M. Mayer, M. Staufer, B.C. Gates, N. Rösch, J. Phys. Chem. B 103 (1999) 5311.
[35] A.A. Davidov, Infrared Spectroscopy of Adsorbed Species on the Surface of Transition Metal Oxides, Wiley, Chichester, 1990.
[36] K. Hadjiivanov, J. Saussey, J.L. Freysz, J.C. Lavalley, Catal. Lett. 52 (1998) 103.
[37] Y.H. Yeom, J. Henao, M.J. Li, W.M.H. Sachtler, E. Weitz, J. Catal. 231 (2005) 181.
[38] A.L. Goodman, G.M. Underwood, V.H. Grassian, J. Phys. Chem. A 103 (1999) 7217.
[39] P.J. Linstrom, W.G. Mallard (Eds.), NIST Chemistry WebBook, NIST Standard Reference Database Number 69, March 2003.
[40] T. Li, W. Minami, H. Kim, Environ. Sci. Technol. 39 (2005) 9665.
[41] M. Haneda, I. Nakamura, T. Fujitani, H. Hamada, Catal. Surveys Asia 9 (2005) 207.
[42] J. Szanyi, J.H. Kwak, R.A. Moline, C.H.F. Peden, Phys. Chem. Chem. Phys. 5 (2003) 4045.

[43] M.J. Harris, E.K.H. Salje, B.K. Guttler, J. Phys. Condens. Matter 2 (1990) 5517.
[44] C. Henriques, O. Marie, F. Thibault-Starzyk, J.-C. Lavalley, Micropor. Mesopor. Mater. 50 (2001) 167.
[45] I.V. Yentekakis, A. Palermo, N.C. Filkin, M.S. Tikhov, R.M. Lambert, J. Phys. Chem. B 101 (1997) 3759.
[46] M.F. Brawn, R.D. Gonzales, J. Catal. 47 (1977) 333.
[47] K. Almusaiteer, S.S.C. Chuang, J. Catal. 184 (1999) 189.
[48] A.M. Venezia, L.F. Liotta, G. Deganello, P. Terreros, M.A. Peña, J.L.G. Fierro, Langmuir 15 (1999) 1176.
[49] G. Li, K. Kaneko, S. Ozeki, Langmuir 13 (1997) 5894.
[50] A. Holmgren, B. Anderson, J. Catal. 178 (1998) 14.
[51] S.J. Schmeig, D.N. Belton, Appl. Catal. B 6 (1995) 127.
[52] E.S. Putna, R.J. Gorte, J.M. Vohs, G.W. Graham, J. Catal. 178 (1998) 598.
[53] C.D. Valentin, G. Pacchioni, S. Abbet, U. Heiz, J. Phys. Chem. B 106 (2002) 7666.